Nanoscale

Check for updates

Capture and electrochemical conversion of CO_2 in molten alkali metal borate−carbonate blends†

Lev Bromberg,[a] Michael P. Nitzsche[b] and T. Alan Hatton (ID) *[a]

A family of blended compositions of molten mixed lithium and sodium borate ($Li_{1.5}Na_{1.5}BO_3$) and eutectic lithium−potassium carbonate ($Li_{1.24}K_{0.76}CO_3$) salts has been introduced as reversible carbon dioxide absorbents and as media for CO_2 electrolysis for carbon conversion. Material properties, temperature effects and kinetics of CO_2 uptake were examined. Li, Na borate can absorb up to 7.3 mmol g^{-1} CO_2 at 600 °C. The blended borate−carbonate compositions are molten in the 550−600 °C temperature range, with viscosity adjustable to within a 10−1000 Pa s window depending on the borate/carbonate ratio. The blends can withstand cyclic temperature and CO_2 pressure swings without significant deterioration of their CO_2 uptake capabilities. Addition of eutectic carbonate into mixed Li, Na borate salts lowers overall CO_2 uptake due to the lower solubility of CO_2 in carbonate. However, addition of the eutectic lowers the temperature of the pressure swing operation and dramatically accelerates the CO_2 uptake during the initial stage of the absorption, potentially enabling a faster cycling. Electroreduction of CO_2 and carbon deposition on a galvanized steel cathode was more effective with increasing carbonate fraction in the molten alkali borate/carbonate blend. Blended borate/carbonate compositions with 50−60% borate content possessed sufficiently high loading capacity for CO_2 and simultaneously enabled maximum carbon product yield and Coulombic efficiency. Most of the recovered carbon product was shown to be in the form of multiwalled carbon nanotube.
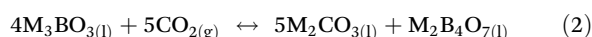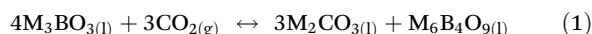
Introduction

Efficient capture and conversion of carbon dioxide (CO_2) is a key pathway toward achieving carbon neutrality of the carbon-producing processes, which is now an imperative accepted worldwide. Among technological innovations in carbon capture, utilization and storage (CCUS) aiming at global warming relief, electrochemical capture and conversion utilizing molten salts appears to be promising.[1–5] The potential for efficient generation of O^{2-} and CO_3^{2-} anions from CO_2 at elevated temperatures and a large operational range for electrochemical oxidation–reduction applications make molten salts an excellent medium for the CCUS processes. Thus far, only metal carbonates and chlorides (and their blends) have been used as molten salt materials with the CO_2 solubility acceptable for electrochemical conversion of CO_2.[1,4–10]

Our group has advanced molten alkali metal borates such as lithium borate (Li_3BO_3) and mixed lithium, sodium borates

as reversible CO_2 sorbents due to their large and temperature-reversible sequestration capacity for CO_2 and acid gases, which generally exceeds the capacity of other molten salts.[11–19] Thermoreversible reactions of the alkali metal borate glasses with CO_2 are well-documented.[11–20] The chemisorption of CO_2 by alkali metal (M) borate M_3BO_3 results in the reversible formation of carbonate (M_2CO_3), metal oxide (M_2O)–boron oxide (B_2O_3) binary compounds, and metaborate (MBO_2) as follows.

$$4M_3BO_{3(l)} + 3CO_{2(g)} \leftrightarrow 3M_2CO_{3(l)} + M_6B_4O_{9(l)} \quad (1)$$

$$4M_3BO_{3(l)} + 5CO_{2(g)} \leftrightarrow 5M_2CO_{3(l)} + M_2B_4O_{7(l)} \quad (2)$$

$$M_3BO_{3(l)} + CO_{2(g)} \leftrightarrow M_2CO_{3(l)} + MBO_{2(l)} \quad (3)$$

$$2M_3BO_{3(l)} + 3CO_{2(g)} \leftrightarrow 3M_2CO_{3(l)} + B_2O_{3(l)} \quad (4)$$

(M = Li, Na, K, *etc.*).

Forward chemical reactions of CO_2 with metal borates occur primarily in the 400–650 °C temperature range and lead to carbon dioxide absorption and formation of metal carbonate salts. The temperature ranges over which carbonate salt forms depend on the metal utilized. The reverse reactions become favored at temperatures above 500–700 °C and result in metal carbonate decomposition and carbon dioxide release.

[a]*Department of Chemical Engineering, Massachusetts Institute of Technology, 77 Massachusetts Avenue, Cambridge, MA 02139, USA. E-mail: tahatton@mit.edu*
[b]*Department of Mechanical Engineering, Massachusetts Institute of Technology, 77 Massachusetts Avenue, Cambridge, MA 02139, USA*
†Electronic supplementary information (ESI) available. See DOI: https://doi.org/10.1039/d2nr03355k

In a concurrent study,[21] we discovered that the alkali metal carbonates that result from the chemisorption of CO_2 by alkali metal borates (reactions (1)–(4)) could subsequently be converted to carbon by electrolysis in a specific temperature range. However, the formation and yield of carbon in the molten borate by CO_2 electrolysis are conditional upon saturation of the melt by CO_2, the formation of carbonate salts (M_2CO_3), and dissociation of these salts leading to the formation of carbonate anions, which are necessary for the electrolytic conversion of CO_2 to carbon:[4–6,10]
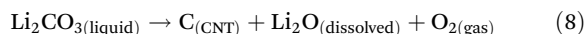
Formation of carbonate ions:

$$M_2CO_{3(molten)} \leftrightarrow 2M^+ + CO_3^{2-} \tag{5}$$

Four-electron reduction of the carbonate ions to carbon on cathode:

$$CO_3^{2-} + 4e^- \rightarrow C + 3O^{2-} \tag{6}$$

Continuous formation of oxygen on the anode:

$$2O^{2-} - 4e^- \rightarrow O_2 \tag{7}$$

Although reactions (5) and (6) do occur with sodium, potassium and alkaline earth carbonates,[9] the production of carbon in the form of CNTs by electrolysis in metal carbonate melts occurs primarily with Li^+ present in the carbonate (Li_2CO_3) and proceeds together with the formation of oxygen and lithium oxide.

$$Li_2CO_{3(liquid)} \rightarrow C_{(CNT)} + Li_2O_{(dissolved)} + O_{2(gas)} \tag{8}$$

The formation of lithium oxide (8) is very important for the lithium carbonate recycling, as Li_2CO_3 is consumed by the electrolysis and needs to be continuously replenished by reaction of excess Li_2O (formed electrolysis product) with the CO_2 supplied:

$$Li_2O_{(dissolved)} + CO_{2(atmospheric, dissolved)} \rightarrow Li_2CO_{3(molten)} \tag{9}$$

However, the melting of lithium carbonate necessary for carbonate ion formation (reaction (5)) occurs at temperatures above 723 °C, whereas the decomposition of lithium carbonate and formation of lithium oxide (Li_2O) is achieved only at temperatures above 1200 °C. These high temperatures are problematic for proper operation, since the presence of Li_2O from lithium carbonate is a condition for CO_2 capture, which is necessary for the reversible mode of CO_2 capture and release using carbonate molten salts (temperature swing). Without the presence of metal oxides in the molten alkali metal carbonates, the capacity of the molten carbonates for CO_2 capture from the environment is low, and therefore, the subsequent electrolytic CO_2 conversion to the value-added carbon products is limited in scale and is inefficient. However, the direct addition of Li_2O to molten lithium carbonate is restricted, because dissolution of solid Li_2O in Li_2CO_3 only occurs at $T >$ 750 °C. When Li_2O is added to Li_2CO_3 at 750 °C, Li_2CO_3 is observed to absorb CO_2 from air; at 550 °C, Li_2CO_3 or its mixture with Li_2O are present in a solid form and Li_2CO_3 will desorb CO_2 into air by decomposition at that temperature,[22]

contrary to the intent of enhancing CO_2 sorption capacity. Therefore, lithium carbonates per se are inefficient as reversible CO_2 sorbents at medium temperatures (below 750 °C) and are commonly replaced by mixed Li, Na, K carbonates as molten salt media in CO_2 electrolysis.[8,10,24,25]

On the other hand, eutectic salt compositions of lithium and sodium and/or lithium and potassium carbonates that possess lower melting temperatures (<750 °C) are well-known.[26,27] Electrochemical carbonate ion reduction and carbon formation/deposition reactions from eutectic alkali metal carbonate melts in the 500–750 °C range have been reported to occur on metallic cathodes made of Ni, Pt, W, Ag, Mo, Al, Cu, and steel, as well as glassy carbon electrodes.[25] Carbon formation has been reported on steel electrodes in mixed melts such as Li_2CO_3–Na_2CO_3 (eutectic mole ratio, 52 : 48) or Li_2CO_3–K_2CO_3 blends (molar ratio, 62 : 38) in the 550–650 °C range.[25,28] In the present work, we aimed to design molten salt compositions that could be applied as both (i) reversible CO_2 capture absorbents and (ii) media for the electroreduction of that captured CO_2 to value-added carbon nanotubes. We surmised that the addition of a eutectic alkali metal carbonate to the alkali metal borates could facilitate electrochemical reduction of CO_2 captured by the molten borates, given that both the borate and carbonate salts can melt and form homogeneous blends in the same preferential temperature range of 550–650 °C. Importantly, potentially deleterious autocausticizing and decarbonization reactions of carbonates by alkali metal metaborate and borates are known to occur in the 900–1000 °C range,[12,29] but can be averted in the target temperature range.

Electrolytic production of carbon nanotubes using molten lithium carbonate compositions can be aided or mediated by the addition of small quantities of metaborates.[30,31] Adding lithium metaborate ($LiBO_2$) into molten $LiCl$–Li_2CO_3 electrolyte at metaborate concentrations up to 1–2 wt% can thermodynamically change the reaction pathway, accelerating the electrolysis and enabling formation of the CO_2-derived products such as CO or CNT at lower cell voltages.[30–32]

Albeit the mechanisms of the carbon nucleation and growth into CNT and other nanostructured materials in the CO_2 electroreduction processes occurring in alkali metal molten carbonates have been subjected to detailed studies,[4–10,30,31] blends of alkali metal borates and carbonates have not been studied at large borates concentrations (>10%). Herein, we describe blended alkali metal borate/eutectic carbonate compositions that can be optimized specifically for the use in carbon capture, utilization and storage (CCUS) processes.

Experimental

General methods

Thermal characteristics and sorbent properties of the salts were analyzed by the weight and heat flow variations of the samples inside a thermogravimetric analyzer (TGA, Q50 or

Q600, both from TA Instruments, Inc., New Castle, DE) or using a differential scanning calorimeter (DSC, Q600 or Discovery DSC 250, TA Instruments). For DSC measurements, heating and cooling ramp scanrates of 10 °C min⁻¹ were applied in the temperature ranges up to 540 °C (Discovery DSC 250) and up to 1200 °C (Q600); DSC samples were sealed in aluminum pans (Discovery DSC 250) and the measurements were conducted in nitrogen atmosphere. TGA heating ramps were conducted on sample exposure to a flow of either 100% CO_2 or N_2. Unless specified otherwise, the mass of sample was 5–10 mg; the gas flow rate was 60 mL min⁻¹. To calculate CO_2 uptake, the fractional weight change on exposure to CO_2 (MW 44.01) was normalized by the sample mass after final pretreatment by N_2 to obtain the CO_2 loading in mmol CO_2 per gram sorbent (Q_{CO_2}, mmol g⁻¹). Temperature ramps were carried out from 200 to 800 °C at varying heating rates. Capacity was defined as certain CO_2 loading after uptake under a CO_2 flow.[17] XRD patterns were obtained by using a 3rd generation Empyrean multipurpose X-ray diffractometer (Malvern PANalytical) equipped with a Cu radiation source and X-ray generator power of 4 kW (max 60 kV, 100 mA) at room temperature. Studied interval was $2\theta = 4$ to 70° and angular resolution, 0.026°. XRD scans within the temperature range from ambient to 600 °C were performed in argon or CO_2 atmosphere using a PANalytical X'Pert Pro instrument with a 1.8 kW sealed X-ray tube source, a Cu target, and a vertical circle goniometer with a radius of 240 mm.

Transmission electron microscopy (TEM) and scanning electron microscopy (SEM) experiments were conducted using a JEOL 2010 Advanced High Performance TEM and JEOL 5910 General Purpose SEM, respectively. Carbonaceous products collected on galvanized steel cathode obtained in the blends' electrolysis at 550 °C were deposited onto TEM gold-coated grids from their suspensions in isopropyl alcohol followed by drying under vacuum. Elemental analysis was performed in an EPA-certified laboratory using inductively coupled plasma-mass spectrometry.

XPS spectra were measured using a PHI Versaprobe II XPS instrument with a scanning X-ray source and a UV lamp (Physical Electronics, Inc., Chanhassen, MN). Prior to taking XPS spectra on electrode surfaces, the original electrode wire was washed by acetone and water followed by drying; the wire that had been used in electrolysis and withdrawn from the molten salt at 550 °C was equilibrated at ambient temperature and then gently washed by water and dried in air; the same electrode was then cleaned off by immersion in a 1% aqueous solution of nitric acid and sonication for 45 min. Peak assignments were performed using built-in instrument software.

Raman spectra of the purified carbonaceous products of the CO_2 electroreduction were measured using a Renishaw inVia Reflex Raman spectrometer (laser excitation wavelength, 532 nm) coupled to a confocal microscope.

ARES-G2 Rheometer with Forced Convection Oven (TA Instruments, Inc.), operating at temperatures up to 600 °C was used with stainless steel parallel plate geometry (40 mm diameter, gap 0.5 mm). Series of single rate viscosity measurements were conducted at 550 or 600 °C at short step times and varying shear rates. Each viscosity datapoint was measured in triplicate.

Salt syntheses

Preparation of alkali metal carbonate. Lithium carbonate (Li_2CO_3, ACS reagent, ≥99%) and potassium carbonate (K_2CO_3, ACS reagent, ≥99%) were both obtained from Sigma Aldrich Chemical Co. Powderous blend of Li_2CO_3 (21.07 g, 0.285 mol) and K_2CO_3 (24.16 g, 0.175 mol) was ground at ambient temperature using mortar and pestle and was dried on air at 350 °C for 8 h in an electric oven. Following cooling, the resulting eutectic Li, K carbonate (62 : 38 mol ratio of lithium and potassium carbonates, nominal composition, abbreviated $Li_{1.24}K_{0.76}CO_3$) was again ground and kept in a sealed container prior to the use.

Preparation of alkali metal borate. Lithium hydroxide (LiOH, 98%), sodium hydroxide (NaOH, ≥98%, anhydrous), and boric acid (H_3BO_3, 99.5%) were obtained from Sigma Aldrich Chemical Co. All water utilized was Mill-Q (Millipore) deionized water. Deionized water (30 mL) was gently added to a powderous mixture of solid LiOH (9.1 g, 0.39 mol), NaOH (15.03 g, 0.39 mol) and H_3BO_3 (15.88 g, 0.26 mol) and the resulting suspension was sonicated for 5 min following by heating at 60 °C while stirring in a sealed bottle. The resulting suspension was allowed to dry at 100 °C on air overnight and the resulting powder was gently ground by mortar and pestle and dried at 400 °C for 4 h. Following cooling, the resulting Li, Na borate (composition, $(Li_{0.5}Na_{0.5})_xB_{1-x}O_{1.5-x}$, $x = 0.75$, abbreviated as $Li_{1.5}Na_{1.5}BO_3$) was again ground and kept in a sealed container prior to the use.

Preparation of blended borate/carbonate compositions. Weighed amounts of carbonate ($Li_{1.24}K_{0.76}CO_3$) and borate ($Li_{1.5}Na_{1.5}BO_3$) were mixed with a spatula, ground by mortar and pestle for 5 min, dried on air in an electric oven for 3 days at 100 °C and then kept in a sealed vial at ambient temperature prior to the use. Each blend was analyzed for water content using thermogravimetric analysis and the borate content (mol%) was then corrected due to the measured presence of hydrate (clathrate) water. The compositions of the borate–carbonate blends are listed in Table 1.

Electrolysis of CO_2 in borate/carbonate blend electrolyte

Electrolysis of CO_2 was conducted using a home-made temperature-controlled tubular glass reactor equipped with furnace,

Table 1 Compositions of preferred borate and carbonate blends. Borate: $Li_{1.5}Na_{1.5}BO_3$; carbonate: $Li_{1.24}K_{0.76}CO_3$

Sample no.	Nominal borate content (mol%)	Borate content corrected (mol%)	Carbonate content corrected (mol%)
1	100	100.0	0.0
2	75	68.9	31.1
3	50	48.3	51.7
4	25	21.4	78.6
5	0	0.0	100.0

Fig. 1 Schematic and photograph of the reactor for molten salt CO_2 electrolysis.

gas inlet/outlet, stainless steel caps, and insulated electrode lines (Fig. 1). The electrode cables were connected to a computer-controlled BioLogic Model SP-101 potentiostat (Biologic, Seyssinet-Pariset, France).

The anode was a nickel crucible composed of 99.5% nickel (nominal volume, 20 mL, Sigma-Aldrich Chemical Co.). A copper coil with a copper wire lead was used as an electrical connector.

The cathode was constructed of hot-dip galvanized steel wire (Fi-Shock WC-14200, G90 coating designation according to ASTM A653; zinc coating layer thickness approximately 18 μm). The cathode was fabricated from a 14 Ga wire made into a disk with area of *ca.* 2 cm². Identical cathodes, but made of 316SS stainless steel wire (McMaster-Carr), or 99% nickel rod (Goodfellow), were used in separate series of experiments.

The details of the electrolysis experiments in this work consisted of the steps described in ESI.†

Coulombic efficiency (C_e, %) was calculated as the percent of applied, constant current charge that was converted to carbon during the CO_2 electrolysis, determined as:[6]

$$C_e \ (\%) = 100 \times M_{exp}/M_{theor} \tag{10}$$

where M_{exp} is the mass of purified carbon product removed from the cathode; $M_{theor} = (Q/nF) \times (12.01$ g C per mol) is the theoretical mass, which is determined from Q, the time integrated charge passed during the electrolysis; $F = 96\ 485$ As mol^{-1} e$^-$ is the Faraday constant, and $n = 4$ e$^-$ mol^{-1} is the reduction number of tetravalent carbons. The mass of carbon product M_{exp} was determined from the total mass of purified dried product multiplied by the mass fraction of total carbon in that given product sample measured by elemental analysis. Standard error for C_e was measured to be 9% in a series of independent experiments.

Results and discussion

Characterization of the molten salt properties

Our choice of the eutectic carbonate ($Li_{1.24}K_{0.76}CO_3$) studied in this paper was predicated on the prior studies demonstrating relatively low melting temperature and concomitant maximum lithium content of that particular carbonate.[26,27] High Li content can be conducive to the enhancement of carbon yield during electrolysis. On the other hand, the Li, Na borate utilized throughout ($Li_{1.5}Na_{1.5}BO_3$) was chosen due to the extensive prior optimization work by our group indicating that this particular composition possessed maximum CO_2 sorption capacity relative to others while maintaining liquid properties and homogeneity even after reaction with CO_2 in the molten state.[17]

Thermal properties of alkali metal borates and their blends with carbonates

Representative TGA and endothermal DSC thermograms on heating of samples of the studied alkali metal borate and carbonate, and their blends in a nitrogen atmosphere are shown in Fig. 2 and 3, respectively. The lithium-containing samples contained varying fractions of crystalline water. Li, K carbonate lost the majority of that water at $T > 130$ °C and showed stability until approximately 700 °C, above which the weight loss began due to decomposition. Eutectic Li, K carbonate ($Li_{1.24}K_{0.76}CO_3$) showed no further weight loss during repeated TGA cycling in the range up to 650–700 °C (data not shown).[28] In comparison, Li, Na borate ($Li_{1.5}Na_{1.5}BO_3$) appeared to be more hygroscopic than the carbonate and lost crystalline water over several stages, above 100, 230, and 400 °C. In the repeated cooling and heating cycles, the borate showed no signs of weight loss at temperatures up to at least 800 °C. The borate–carbonate blend pre-treated at 600 °C in nitrogen atmosphere lost less than 1% of its weight over a broad range of temperatures (Fig. 2). Hence, the prepared blends showed promise as
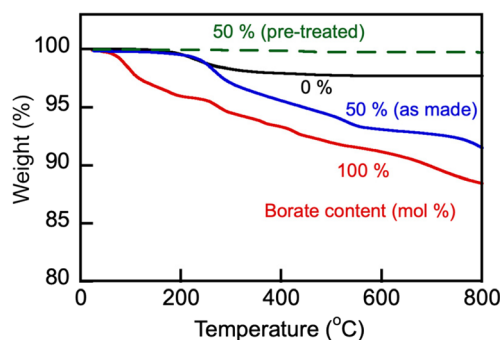

Fig. 2 TGA heating ramp (10 °C min^{-1}) of as-made carbonate ($Li_{1.24}K_{0.76}CO_3$), borate ($Li_{1.5}Na_{1.5}BO_3$) and as-made and pre-treated blend (1 : 1 mol/mol, sample no. 3 in Table 1) in nitrogen atmosphere. The blend sample was pre-treated by its equilibration at 600 °C in N$_2$ atmosphere for 1 h. Numbers stand for nominal initial content of borate (mol%) in the samples.
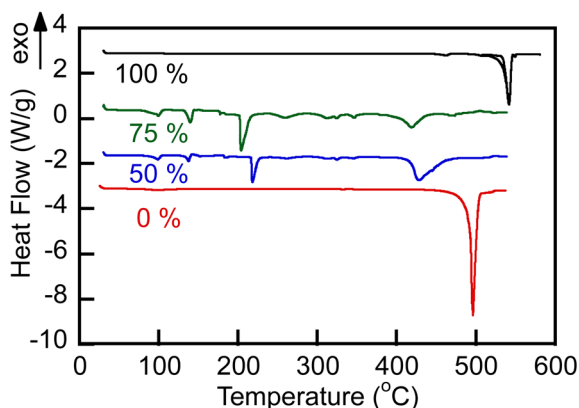
Fig. 3 DSC melting endotherms on 10 °C min^{-1} heating of the carbonate ($Li_{1.24}K_{0.76}CO_3$) and borate ($Li_{1.5}Na_{1.5}BO_3$) and their blends in nitrogen atmosphere. Numbers indicate nominal initial content of borate (mol%) in the blends. Endotherms were shifted along the heat flow axis for the presentation clarity, while preserving the original scale. Solid and dashed lines represent endotherms obtained using a Discovery DSC 250 (sealed pans) and Q600 (open to nitrogen atmosphere), respectively.

Fig. 4 Diffraction patterns of a blend of Li, Na borate ($Li_{1.5}Na_{1.5}BO_3$) and Li, K carbonate ($Li_{1.24}K_{0.76}CO_3$) (1 : 1 mol/mol), as-made (a), the same blend reacted with CO_2 at 550 °C, quenched and measured at 25 °C (b) and the same reacted blend as in (b), but re-melted with XRD measured at 550 °C (c). Asterisks mark peaks matching planes of tetragonal Li and Li, Na tetraborate crystalline phase at 20.4°.[33] Ovals mark patterns pertaining to lithium metaborate ($LiBO_2$). Squares designate Li_2CO_3 and Li, $NaCO_3$ crystal patterns. Crystal pattern references: International Central Securities Depository (ICSD) and JCPDS (Joint Committee on Powder Diffraction Standards) or ICDD (International Centre for Diffraction Data) as follows. ICDD 04-009-3631; ICDD 04-009-6084; ICSD 419673; ICSD 415327; ICSD 65930; ICSD 419673; ICSD 415327; ICSD 16568; ICSD 37060; ICSD 200891.

stable regenerable molten media for repeated temperature cycling operations.

DSC traces showed (Fig. 3) that all studied salt compositions melted at temperatures below 550 °C, demonstrating sharp melting endotherms. Melting of the eutectic carbonate $Li_{1.24}K_{0.76}CO_3$ was centered at 496 °C, in excellent agreement with the previously reported data.[26,27] Borate $Na_{1.5}Li_{1.5}BO_3$ melting occurred at 539 °C. The borate–carbonate blends (B/C molar ratios 1 : 1 and 3 : 1), as prepared, contained residual hydrate water and melted above 450 °C. The blends recrystallized on cooling at temperatures below 400 °C (cooling exotherms are not shown in Fig. 3). Melting in nitrogen atmosphere enabled removal of crystalline water. Importantly, all materials studied were observed to be consistently liquid at 550 °C under nitrogen atmosphere or in air.

However, due to the reactivity of the borate with CO_2 and its chemical conversion to metaborate while generating alkali metal carbonate, formation of multiple metastable phases upon reaction of the borate component with CO_2 was possible.[17] We thus examined formation of the crystalline phases, if any, in the borate/carbonate blend upon its uptake of and reaction with CO_2 in cooling and subsequent re-melting of the reacted blend (Fig. 4). Reaction was conducted on a platinum pan in 100% CO_2 at 550 °C for 3 h and then the reacted blend sample was cooled at 5 °C min^{-1} to ambient temperature in a CO_2 atmosphere and the recrystallized material was placed on a zero-background silicon wafer, where XRD was measured at 25 °C (b) and 550 °C, also in a CO_2 atmosphere (c). It was observed that upon reaction of the borate component with CO_2 (eqn (3), the reacted blend re-melted and demonstrated the absence of any crystalline phases at 550 °C (Fig. 4(c)). This is important for the heating–cooling cycling (temperature swing operation) of the blends in their utilization as regenerable CO_2 sorbents.[17]
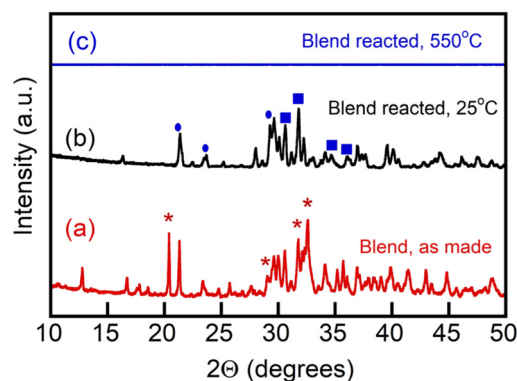
Viscosity of alkali metal borate/carbonate blends

Alkali (e.g., primarily Li) meta- and tetraborates have been used extensively in a number of applications, primarily as fluxing components for X-ray fluorescence (XRF), atomic emission spectrometry and related analytical techniques.[34,35] Molten lithium tetraborate generally possesses a high viscosity and tends to solidify as a glass under small temperature gradients.[35–37] The viscosity of molten lithium borates under temperature gradients is determined by the ratio of optically opaque crystalline matrices and amorphous phases, both with the chemical formula of $Li_2B_5O_9$.[35–41] The amorphous motif can have the structural form of a single tetrahedral boron connected to four oxygen atoms. The oxygen atoms are connected to the trigonal boron species to form a ring with the chemical formula of B_3O_3. In contrast to the alkali metal borates, alkali metal carbonate melts are extremely fluid and the viscosity of the Na_2CO_3, K_2CO_3, and Li_2CO_3 liquids measured by rotational viscometers is on the order of 3–20 mPa s in the 750–1000 °C range and demonstrates Arrhenian behavior.[42–44]

In the present work, we were interested in the behavior of blends of the two distinct classes of alkali metal salts, i.e., borates and carbonates, in their molten state under moderate shear stresses and in the lowest temperature range (550–600 °C), wherein both salts are molten. To the best of our knowledge, no reports on the viscosity of blended borate–carbonate melts is available, albeit the viscosities of individual $Na_xB_{1-x}O_y$ (x = 0.75) and $(Li_{0.5}Na_{0.5})_xB_{1-x}O_y$ (x = 0.75) borates in the molten state at 600 °C have been reported by our group.[12]
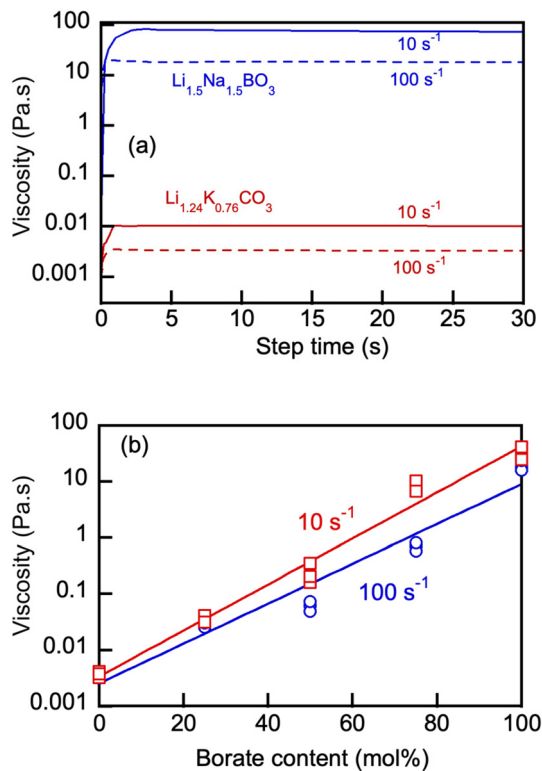
Fig. 5 (a) Rotational viscosity of Li, Na borate ($Li_{1.5}Na_{1.5}BO_3$) and eutectic Li, K carbonate ($Li_{1.24}K_{0.76}CO_3$) measured at 550 °C and at constant shear rates of 10 and 100 s^{-1} and the effect of borate concentration on viscosity of Li, Na borate ($Li_{1.5}Na_{1.5}BO_3$) and eutectic Li, K carbonate ($Li_{1.24}K_{0.76}CO_3$) blends at 550 °C and at shear rates of 10 and 100 s^{-1} (b). Numbers denote nominal initial borate concentration (mol%) in the blend. Straight exponent fits ($R^2 > 0.98$) are shown to guide the eye only.

Fig. 5(a) shows representative rotational viscosity measurements of the Li, Na borate ($Li_{1.5}Na_{1.5}BO_3$) and eutectic Li, K carbonate ($Li_{1.24}K_{0.76}CO_3$) at 550 °C at constant shear rates of 10 and 100 s^{-1}. Pronounced shear-thinning behavior of both molten salts was evident in these measurements, with the borate's viscosity being 3 orders of magnitude larger than that of the carbonate at that temperature. The viscosity of $Li_{1.5}Na_{1.5}BO_3$ measured at constant 100 s^{-1} and 550 and 600 °C was 32 ± 8 ($n = 3$) and 14 ± 5 Pa s ($n = 3$), respectively, which corresponded well with the previously reported data on Li, Na borate at 600 °C.[12]

Variation of the borate content in the blends (Fig. 5(b)) appeared to produce a pronounced effect on the blend viscosity, ranging over 3 orders of magnitude. The results show that eutectic carbonates act as an efficient diluent for the molten alkali metal borates and the blend's viscosity can be adjusted as required for proper handling, pumping, circulation and other operations requiring transport of molten salts at high temperatures, especially in heat transfer and electrolysis applications.

CO$_2$ uptake by alkali metal borates and their blends with carbonates

The parameters of CO$_2$ uptake by molten salts were examined with Li, Na borate, $Li_{1.5}Na_{1.5}BO_3$ and its representative blend with the eutectic Li, K carbonate under study, $Li_{1.24}K_{0.76}CO_3$ (Fig. 6). The uptake of CO$_2$ (Q, mmol g^{-1}) during temperature was ramped at a very slow rate of 0.33 °C min^{-1} under a flow of 100% CO$_2$. Prior to the temperature ramp in CO$_2$, the samples were first purged of water and adsorbed air by exposing them to the N$_2$ flow and ramping the temperature to 600 °C at 5 °C min^{-1} and then allowing to equilibrate, also under N$_2$ flow, at 200 °C for 1 h. The slow heating rate enabled precise determination of temperature of the CO$_2$ uptake onset (T_{on}) and the CO$_2$ uptake maximum (Q_{max}).

The uptake of CO$_2$ by Li, Na borate increased dramatically once the temperature was raised to the onset temperature (T_{on}) of 492 °C. After the sharp increase of the CO$_2$ uptake at T_{on}, the uptake rapidly reached maximum load capacity (Q_{max}, ~7.1 mmol g^{-1}) at T_{max} = 552 °C and then after a short plateau started to decrease at higher temperatures starting at 563 °C. Similar behavior was observed with the borate–carbonate blend. However, the presence of $Li_{1.24}K_{0.76}CO_3$ carbonate in the blend caused a dramatic temperature shift in T_{on} to 395 °C, and the uptake became two-step, increasing first at >395 °C and then more significantly around 460 °C before a final rapid increase, plateau and subsequent decrease. The shift of the T_{on} values in the presence of carbonate in the blend is certainly due the existence of the Li, K carbonate crystals left in the blend after melting and recrystallization that preceded the CO$_2$ uptake. All crystals are molten above 530 °C (compare with Fig. 4). The Li, K carbonate crystals melt at temperatures much lower than those of the individual borate $Li_{1.5}Na_{1.5}BO_3$ (compare with Fig. 3); the onset of glass transition and melting and the existence of mobile and liquid phases in the salt enables rapid gas–liquid mass exchange and
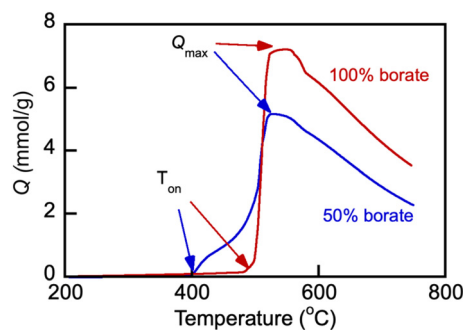

Fig. 6 CO$_2$ uptake by Li, Na borate ($Li_{1.5}Na_{1.5}BO_3$) and its eutectic Li, K carbonate ($Li_{1.24}K_{0.76}CO_3$) blend (borate/carbonate ratio, 1 : 1 mol/mol, sample no. 3 in Table 1) under 60 mL min^{-1} flow of 100% CO$_2$ at a heating rate of 0.33 °C min^{-1}. The CO$_2$ loading (Q, mmol g^{-1}) was calculated as a sample weight fraction ($10 \times W_f$) gained on the exposure to the CO$_2$ flow, normalized by the molar mass of CO$_2$ (44.01 g mol^{-1}). Arrows show the temperature datapoint at which the CO$_2$ uptake was measured to be at maximum (Q_{max}); T_{on} is the temperature of the CO$_2$ uptake onset. Numbers indicate nominal initial borate content.

absorption of CO_2 by the melt, which explains the significantly lower T_{on} in the blend *vs.* that in pure borate.

Fig. 7 shows the effect of varying borate/carbonate blend composition on the CO_2 uptake under a flow of 100% CO_2 at a constant heating rate of 5 °C min^{-1}. The T_{on} scaled with the heating rate (not shown).

As is seen in Fig. 7(b), the addition of eutectic $Li_{1.24}K_{0.76}CO_3$ carbonate to $Li_{1.5}Na_{1.5}BO_3$ borate under study lowered the Q_{max} of the blend because the carbonate's ability to physisorb CO_2 in the studied temperature range is low and does not exceed approximately 0.2 mmol g^{-1}. The Q_{max} values increased linearly with the overall borate concentration. However, both T_{on} and T_{max} significantly decreased with the carbonate addition, which indicates that the blends can be operated as reversible absorbents at lower temperatures than pure borates, which is beneficial.

CO_2 absorption in pressure swing cycling operation

Our group discovered that molten alkali metal borates act as reversible liquid absorbents for CO_2 capture in the medium temperature range of 550 to 600 °C, with regenerability over multiple absorption–desorption cycles under both temperature- and pressure-swing operations.[12,17] Such behavior of the

molten borates in a cyclical absorption–desorption process was ascribed to the "instantaneous" formation of carbonate salts and their subsequent dissociation resulting in carbonate ions being present in the borate without the diffusional transport restrictions imposed by solid product layers characteristic of solid adsorbents.[11–19]

In the present work, we set out to (i) ascertain whether such cycling would be possible with the borate/carbonate blends, and moreover, (ii) establish whether the carbonate salt added to the borate salt prior to any CO_2 chemisorption, would change the kinetics of the CO_2 upload and desorption.

For the direct comparison, we chose to study a Li, Na borate $(Li_{1.5}Na_{1.5}BO_3)$ and eutectic Li, K carbonate $(Li_{1.24}K_{0.76}CO_3)$ blend (borate/carbonate ratio, 1 : 1 mol mol^{-1}) as representative examples. Both the borate and the blend have been shown to be liquid at 550 °C (Fig. 3 and 4), and hence, the pressure swing cycling was performed at that temperature. The results shown in Fig. 8 demonstrate that both the borate salt alone and its blend with eutectic carbonate exhibited reversible uptake-desorption of CO_2 in the pressure swing operation, within the span of at least 22 cycles. The results were quanti-
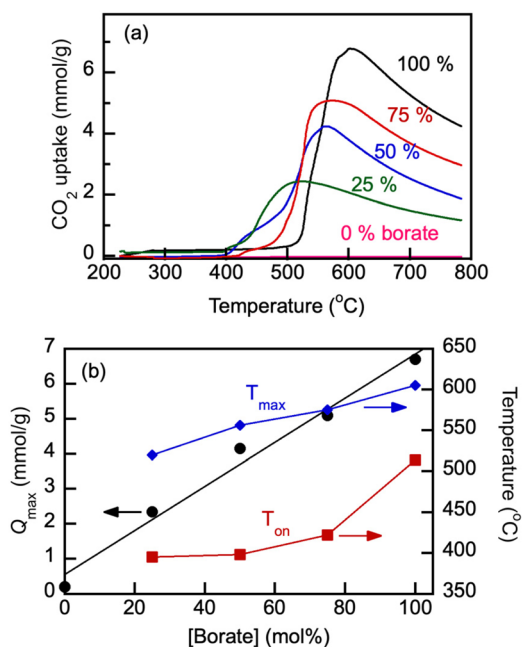

Fig. 7 CO_2 uptake (Q, mmol g^{-1}) by molten borate/carbonate blends under the 60 mL min^{-1} flow of 100% CO_2 at a heating rate of 5 °C min^{-1} (a) and dependencies of the maximum CO_2 loading (Q_{max}), temperature of the onset of the loading increase (T_{on}), and the temperature of the maximum CO_2 loading (T_{max}) on nominal content of Li, Na borate, in the borate/carbonate blends (b). In the TGA experiments, the blends were first purged of water and CO_2 by exposing them to N_2 flow and ramping the temperature to 600 °C at 5 °C min^{-1} and then allowing to equilibrate, also under N_2 flow, at 200 °C for 1 h. The CO_2 loading was calculated as a sample weight fraction gained on the exposure to the CO_2 flow, normalized by the molar mass of CO_2 (44.01 g mol^{-1}). Numbers indicate nominal initial content of borate (mol%) in the blends.
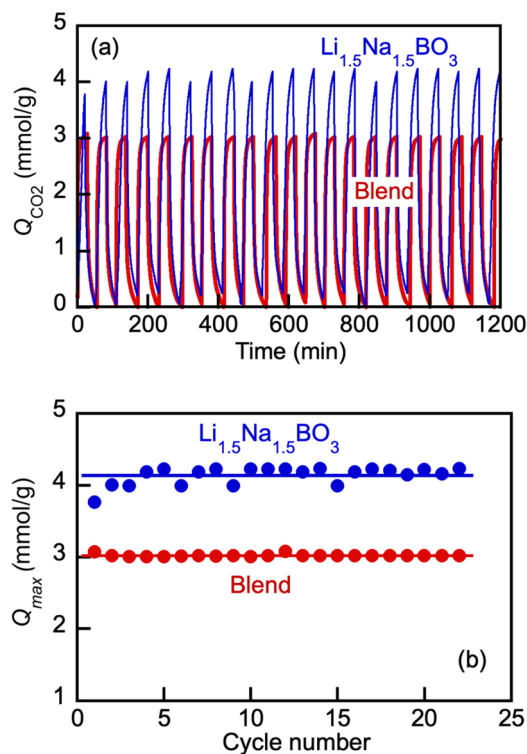

Fig. 8 Effect of cycling on CO_2 uptake by molten Li, Na borate $(Li_{1.5}Na_{1.5}BO_3)$ and eutectic Li, K carbonate $(Li_{1.24}K_{0.76}CO_3)$ blend (borate/carbonate ratio, 1 : 1 mol/mol) (a) and maximum CO_2 loading in each cycle at t_{cycle} = 30 min (Q_{max}, mmol g^{-1}) *vs.* cycle number (b). Cycling was conducted *via* pressure swing operation on repeated switching of the gas stream between 100% CO_2 (pCO_2 = 1 bar) and 100% N_2 (pCO_2 = 0 bar) at 550 °C. Cycle consisted of alternating 30 min of CO_2 flow followed by nitrogen flow (60 mL min^{-1}) for 30 min. The salt samples (6 mg) were evenly spread at the bottom of a platinum pan; temperature 550 °C throughout.

fied with Q_{max} values defined at the end of each sorption cycle (t = 30 min after the instance of the switch to the CO_2 flow) (Fig. 8(b)). As is seen, after the initial 3–4 cycles, the Q_{max} reached constant values of approximately 4.2 and 3.1 mmol g^{-1} for the borate and the blend, respectively. The lower Q_{max} values for the blend *vs.* borate alone are expected (compare with Fig. 7). Importantly, however, the blend did behave as a reversible liquid sorbent. Encouraging by this observation and armed with the knowledge of the dilution effect of the carbonate on the blends' viscosity (Fig. 5), we proceeded to a comparative study of the kinetics of the CO_2 uptake by the borate alone and by the blend in the pressure swing operation.

Detailed comparison of typical CO_2 uptake kinetics in one cycle of the cyclical pressure swing operation shows dramatic differences between the pure borate and the blend kinetics (Fig. 9). Herein, the uptake (Q) is presented *via* the degree of conversion $\alpha = Q/Q_{max}$; wherein Q_{max}, mmol g^{-1}, is the maximum CO_2 loading in the cycle at t_{cycle} = 30 min.

Fig. 9(b) shows dramatic differences in the kinetics of the CO_2 uptake between pure borate and its blend with carbonate. The blend absorbed CO_2 very rapidly at the very beginning of the cycle, with high degrees of conversion reached within 1–2 min, whereas with the pure Li, Na borate the initial rate of absorption was low, starting to accelerate at $t > 0.6$ min, which was followed by gradual deceleration of the CO_2 uptake at $t > 15$ min. Analogous results with $Li_{1.5}Na_{1.5}BO_3$ have been previously obtained at 600 °C by our group.[12] The S-shaped uptake kinetics (slow induction rate-acceleration-leveling off period) can be explained by the initial lag time required for dissolution of CO_2 to accumulate carbonate ions (CO_3^{2-}) in the viscous molten borate oxides at sufficient levels to exceed the supersaturation threshold for nucleation and growth of crystal nuclei to form solid Li, Na carbonate particles (LiNaCO$_3$). In the molten borate–carbonate blend, the carbonate ions are present prior to the onset of the CO_2 uptake and hence, the initial uptake reaches high degrees of conversion.

The overall kinetics of the CO_2 uptake by the molten salts with the nucleation and growth of the carbonate crystalline particles, which can eventually form diffusional barriers for further uptake can be qualitatively described by considering the time intervals over which the uptake rate changes separately.[12,45,46]

The initial CO_2 uptake can be described by the pseudo first-order reaction kinetics:[12,45]

$$-\frac{dQ}{dt} = k_1 Q, \quad \text{or after integration,} \quad -\ln(1-\alpha) = k_1 t \quad (11)$$

where $\alpha = Q/Q\_max$.

The kinetics presented in Fig. 9(b) in terms of eqn (11) highlights dramatic differences in the initial uptake rate by the pure borate $Li_{1.5}Na_{1.5}BO_3$ and its blend with carbonate. The blend started absorbing CO_2 instantly and reached high degrees of conversion ($\alpha > 0.7$) at 0.6 min, whereas pure borate showed an induction lag time before starting to uptake CO_2. The pseudo-first reaction rate constant in the case of the blend
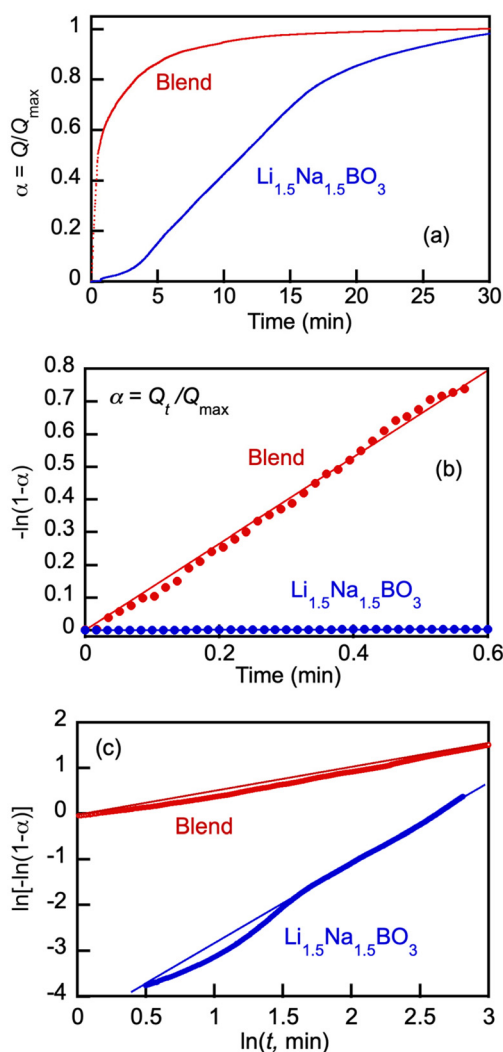

Fig. 9 Typical CO_2 uptake kinetics in one cycle of the cyclical pressure swing operation at 550 °C (a), initial kinetics of CO_2 uptake by Li, Na borate ($Li_{1.5}Na_{1.5}BO_3$) and its blend with eutectic Li, K carbonate ($Li_{1.24}K_{0.76}CO_3$) (borate/carbonate ratio, 1:1 mol/mol) (blend) presented in terms of eqn (11) (b), and variation of CO_2 conversion degree by Li, Na borate its blend presented in double logarithmic plot of the Avrami–Erofeyev equation (eqn (12)) for CO_2 uptake by over the time period of 0.6 min < t < 15 min (c). The data is expressed *via* the degree of conversion $\alpha = Q/Q_{max}$; wherein Q_{max}, mmol g^{-1}, is the maximum CO_2 loading in the cycle at t_{cycle} = 30 min. Molten salts are Li, Na borate ($Li_{1.5}Na_{1.5}BO_3$) and its blend with eutectic Li, K carbonate ($Li_{1.24}K_{0.76}CO_3$) (borate/carbonate ratio, 1:1 mol/mol) (blend). Straight lines with R^2 > 0.98 goodness-of-fit for the linear regressions (eqn (11)–(13)) are shown.

(k_1 = 1.4 min^{-1}) was 250–300-fold higher than that with pure borate ($k_1 \sim 5 \times 10^{-3}$ min^{-1}).

The changes in the CO_2 uptake rate after the initial period (0.6 < t < 15 min) are described by the well-known Avrami–Erofeev nucleation and nuclei-growth model:[12,45–48]

$$-\ln(1-\alpha) = k_2 \cdot t^n; \quad n = p + m \quad (12)$$

where m refers to a dimensional number related to the nuclei growth, p is a nucleation occurrence constant, and k_2 is the reaction rate constant.

Fig. 9(c) shows a logarithmic plot where kinetics of the borate and blend in the $0.6 < t < 15$ min period are presented in terms of eqn (12). The rate of the CO_2 uptake increased with the borate and significantly slowed down with the blend, probably due to the nucleation and growth of crystals as a result of CO_2 reaction with the borate component that is faster in pure Li, Na borate than in the blend when the borate was diluted by carbonate. The k_2 estimates from the linear regression fits (Fig. 9(c), $R^2 > 0.99$) for the borate and blend are 1.9 and 0.6, respectively.

The linearity of the plots in Fig. 9(b) (eqn (11) indicates that the uptake rate was controlled by a second order reaction, possibly through the coordination of double alkali-metal ions to stabilize the carbonate ions forming in the molten boron oxide.[12]

After approximately 15 min, the CO_2 uptake by both borate and the blend further slowed down, attributed to the approaching saturation of the boron oxide melt by the formed carbonates at longer times, and high conversion degrees ($\alpha > 0.8$) observed in the reversible reactions of the carbonate formation and decomposition.

In summary, we have observed that the Li, Na borate and borate/carbonate blends can be applied as reversible molten absorbents of CO_2, without a significant deterioration in the absorption (capture) capacity over many cycles of the pressure swing operation. Addition of carbonates to the molten carbonate lowers overall CO_2 uptake due to the lower sorption capacity of carbonate at the temperatures studied. However, the addition of eutectic carbonates to the molten Li, Na borate lowers the melt viscosity and enables lowering of the temperature of the pressure swing operation as well as dramatically accelerates the CO_2 uptake during the initial stage of the cycle.

Electroreduction of CO_2 in molten alkali metal borate/carbonate blends

In order to conduct CO_2 electrolysis in molten Li, Na borate/Li, K carbonate blends, the choice of the cathode and anode (surfaces from which electrons flow into and from, respectively) is very important. Our concurrent experiments indicated that the molten Li, Na borate can be reliably contained within metallic containers while ceramic crucibles were either damaged by the molten borate or cracked at temperatures of 600 °C.[21] Metals, and in particular, nickel, have been used previously as anode materials in CO_2 electrolysis in molten alkali metal carbonates.[7,49–52] Nickel is readily oxidized in the presence of the molten salt, but the formed nickel oxide layer protects the deeper nickel layers from further oxidation; moreover, nickel oxide is sufficiently conductive that it does not impede the flow of electrons from the anode.[53] Therefore, we chose nickel crucibles to serve as anodes. The cathode employed herein consisted of galvanized steel wire. Galvanized steel is an inexpensive material that in our experiments with alkali metal borates, produced carbon in the form of CNTs.[21] The zinc

layer alloyed with the steel wire *via* hot-dip processes[54] plays a significant role in the CO_2 electrolysis in molten alkali metal carbonates.[55]

During electrolysis, the cathode was coated by carbon deposits that could be readily removed mechanically by sonication in acidic aqueous solution, resulting in colloidally stable suspensions. The removed material was dialyzed against excess aqueous solution and lyophilized for further characterization (see Experimental). The processes occurring on the galvanized steel electrode that underwent various changes during the process of CO_2 electrolysis and then removed from the melt were elucidated using XPS spectroscopy (Fig. 10). Peaks belonging to zinc (Zn $2p_{3/2}$ at 1021 eV, Zn LMM Auger peak centered at 498 eV, *etc.*) and the Zn–O bond in the ZnO matrix centered at 530 eV (ref. 56) (Fig. 9a) disappeared as the electrode was coated by the carbonaceous material during electrolysis (B) and when that carbonaceous layer was mechanically removed, peaks belonging to the underlying iron of the bare steel layer (Fe $2p_{3/2}$ at 711 eV of Fe–O and others), appeared (C). These results clearly show that the zinc coating on the galvanized steel electrode melted at $T > 420$ °C and then dissolved into the molten salt electrolyte, where it co-nucleated with the forming carbon nuclei, accelerating their aggregation, growth and subsequent assembly into carbonaceous material.[7,10,47]

Electrochemical processes occurring during CO_2 electrolysis in molten alkali metal carbonates serving as electrolytic media have been studied extensively by cyclic voltammetry (CV).[22,23,25] There have been no such reports on CO_2 electrolysis in molten borate or borate/carbonate blends, which prompted our interest in such examination. Fig. 11 shows voltammograms obtained in 3 consecutive scans with a representative borate/carbonate blend.

In Fig. 11, CRE denotes carbonate reference electrode (standard potential *vs.* reference CO_2 oxidation reaction is $E° = 0$ V). In our control experiment conducted under air purge, a sys-
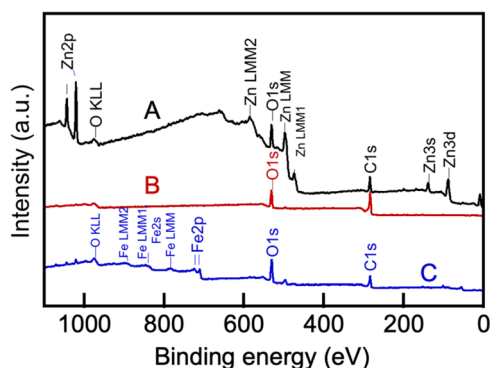

Fig. 10 XPS spectra of the original galvanized steel electrode (A), the same electrode utilized in the CO_2 electrolysis at 550 °C in molten Li, K borate/Li, Na carbonate (1 : 1 mol/mol) blend (B), and the same electrode after cleaning its surface of the CNT deposited during the electrolysis (C). For electrolysis conditions, see Experimental.

Fig. 11 Cyclic voltammograms (CV) of a galvanized steel cathode in a molten borate and carbonate blend (nominal borate: carbonate mol ratio, 1 : 1). Borate: $Li_{1.5}Na_{1.5}B_2O_3$; eutectic Li, K carbonate: $Li_{1.24}K_{0.76}CO_3$. Anode: nickel crucible; temperature: 550 °C. The potential scan started cathodically from 0 V, and the reduction and oxidation sweep directions are shown by arrows (IUPAC convention). Solid blue and dotted red lines show three consecutive scans (scanrate, 10 mV s^{-1}) measured under nitrogen and CO_2 purge, respectively. Designations A and C stand for anodic and cathodic peak potentials, respectively.

temic −0.131 V shift was observed due to the electrochemical cell parameters and conditions relative to the standard potential $(E^{\circ}_{900} = 0\,V)$ characteristic of the carbonate ion oxidation in molten carbonates:[57]

$$CO_3^{2-} \rightarrow CO_2 + 0.5O_2 + 2e^- \qquad (13)$$
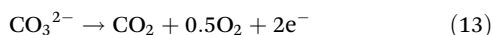
Reaction (13) is indicated by A1 in Fig. 11. The observed formation of black coating on the anode interior is attributed to the nickel oxidation reaction on the anode-melt interface with the reported standard potential $E^{\circ}_{900} = 0.697\,V$:[58,59]

$$Ni^0 + CO_3^{2-} \rightarrow NiO + CO_2 + 2e^- \qquad (14)$$

Reaction (14) is indicated by A2 on the oxidation scan in nitrogen atmosphere in Fig. 15. Lower oxidation currents are observed on the initial scan. Numerous prior studies reported a variety of reduction reactions for nickel compounds (C1) in the presence of neutral gas or carbon dioxide:[58–62]

$$NiO + 2e^- \rightarrow Ni^0 + O_2^-; \quad E^{\circ} = -1.50\,V \qquad (15)$$

During the cathodic reduction, at potentials in the −1.2 to −0.7 V range nickel oxide dissolves, forming complexes of nickel and carbonate ions. These complexes are reduced to nickel and carbonate ions; the formed nickel is then oxidized in the following anodic scan, at potentials in the 0.7 to 1.2 V range.[60,62]

The electrochemical processes occurring with nickel and nickel oxide can be considered side reactions, whereas the reactions of electrodeposition of carbon by CO_2 electrolysis are our target product reactions, which will be discussed next. Important deposition potentials of alkali and alkaline earth metals *via* reactions (16) and carbon through reac-

tions (17) in their own molten carbonate salts are well-known.[23,25]

Electrochemical deposition of metal:

$$2M_2CO_3 \rightarrow 4M + 2CO_2 + O_2 \quad (M = Li, Na \text{ or } K) \qquad (16)$$
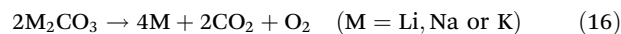
Deposition of carbon *via* carbonate salt decomposition:

$$3M_2CO_3 \rightarrow C + 3M_2O + 2CO_2 + O_2 \qquad (17)$$

In our experiments with borate/carbonate blends in a nitrogen atmosphere, carbon was produced by cathodic reduction of the carbonate anions (reaction eqn (6)) formed by dissociation of the molten alkali metal carbonates (indicated as C2 in the −2.3 V range in Fig. 11). Carbon was deposited on a galvanized steel cathode in significant quantities, along with deposition of alkali metals and boron. The processes of deposition are indicated by C3 in Fig. 11.

In the presence of the Li, Na borate in the borate/carbonate blend (Fig. 11), borate anions (BO_3^{3-}) formed by dissociation of the borate in the molten salt can mediate the CO_2 capture and subsequently, lead to enhanced chemisorption:

$$BO_3^{3-} + CO_2 \leftrightarrow CO_3^{2-} + BO_2^- \qquad (18)$$
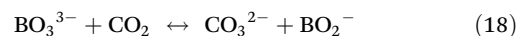
Borate anions also contribute to the metaborate and oxygen anion generation by the molten salt:[31]

$$BO_3^{3-} \leftrightarrow BO_2^- + O^{2-} \qquad (19)$$

Hence, in the presence of the Li, Na borate, the formation of carbonate anions needed for CO_2 electroreduction is augmented, which in turn leads to carbon deposition on the cathode at lower cathodic potentials:

$$CO_3^{2-} + 4e^- + 3BO_2^- \rightarrow C + 2BO_3^{3-} \qquad (20)$$
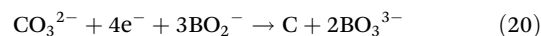
corresponding to the carbonate electroreduction under CO_2 atmosphere in the −1.4 to −1.2 V range and carbon/metal deposition in the −1.8 to −1.5 V range as indicated by C4 and C5, respectively, in Fig. 11. Electroreduction processes in eqn (20) (C4) can be seen as transient, as their peak potentials were lowered with the number of scans, indicating that the majority of the dissolved CO_2 was electroreduced.

The temperature of the electrolysis process with the borate/carbonate blends was fixed at 550 °C, at which the blends exhibited maximum CO_2 uptake at slow rates of heating (Fig. 6). In all experiments, the molten electrolyte was equilibrated with the CO_2 flow prior to the onset of the electrolysis at 550 °C.

The results of the electrolysis conducted at 550 °C in a series of experiments in which the molten salt composition was varied are shown in Fig. 12. The Coulombic efficiency (C_e) results based on the yield of carbon are overlapped with the maximum CO_2 uptake values of the corresponding blend compositions at 550 °C (Q_{max}) measured in TGA experiments. Coulombic efficiency was close to 100% in eutectic Li, K carbonate without the borate added, as expected with galvanized steel cathodes.[24,25] The yield of carbon in the initially pure Li, K borate at 550 °C was approximately 18% in the borate alone,
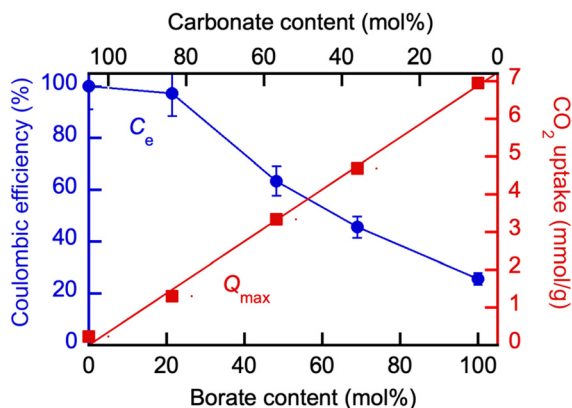
Fig. 12 Effect of the molten borate/carbonate blend composition on the Coulombic efficiency (C_e) of the CO_2 electrolysis and maximum CO_2 uptake (Q_{max}) at 550 °C. Borate: $Li_{1.5}Na_{1.5}B_2O_3$; eutectic Li, K carbonate: $Li_{1.24}K_{0.76}CO_3$. For Q_{max} determination detail, see legend to Fig. 6.
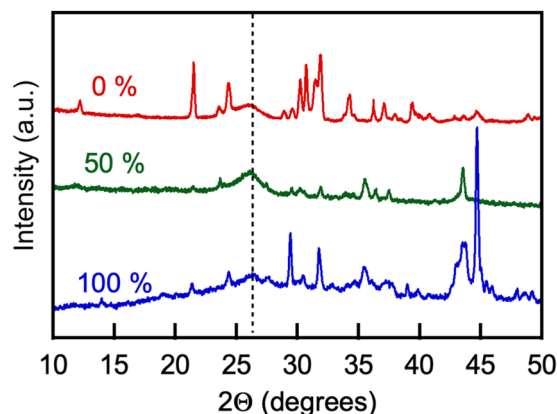

Fig. 13 Representative XRD patterns of the products of CO_2 electrolysis conducted in molten Li, K carbonate ($Li_{1.24}K_{0.76}CO_3$ nominal content of borate, 0 mol%) in borate/carbonate blend (nominal molar carbonate/borate ratio, 1 : 1), and in Li, Na borate ($Li_{1.5}Na_{1.5}B_2O_3$, nominal content of borate, 100 mol%). Borate: $Li_{1.5}Na_{1.5}B_2O_3$; eutectic Li, K carbonate: $Li_{1.24}K_{0.76}CO_3$. Temperature: 550 °C. Cathode: galvanized steel, anode: Ni crucible. Current density on the cathode: 120 mA cm^{-2}. Other conditions are described in Experimental. Numbers stand for nominal molar borate content; dotted vertical line shows graphitic peaks at 26.2 degrees.

but could be improved by the addition of carbonate $Li_{1.24}K_{0.76}CO_3$ to the blend (Fig. 12). On the other hand, at 20% of the borate added into carbonate, the Coulombic efficiency of the carbon production was close to 100% while the CO_2 uptake was a lot higher than Q_{max} in pure Li, Na carbonate and sufficient for the high yield of the carbon product.

The opposing C_e vs. Q_e trends enable performance optimization via the blend composition to trade off the equilibrium CO_2 sorption (capture) uptake with the yield of carbonaceous product during CO_2 electrolysis as measured by Coulombic efficiency.

Structure of the products of CO_2 electrolysis in molten borate/carbonate blends

The products of the CO_2 electrolysis were recovered and purified (see Experimental). Elemental analysis for carbon content in the products varied significantly from approximately 20 to 98 wt% depending on the extent of product purification by washing; concentrations of lithium, zinc and nickel varied in the 0.2 to 3.5 wt%, 0.01–2 wt%, and 0.1–1.5 wt% ranges, respectively.

Fig. 13 shows a general view of the powder XRD pattern of the products of CO_2 electrolysis collected on the galvanized steel cathodes. The broad peaks centered at $2\Theta = 26$–26.2° observed in the XRD patterns of the electrolysis products obtained with either molten Li, Na borate or Li, K borate or their blends were prominent. The (100) crystal peaks are characteristic of multiwall carbon nanotubes and correspond to a d-spacing between graphene sheets (CNT wall layers) of 3.42–3.46 Å.[63–65] The XRD patterns of the electrolysis products also featured peaks at $2\Theta = 21.3$, 30.6, and 31.8°, characteristic of the lithium carbonate admixtures that were not removed from the products in the process of purification.[66] XRD pattern peaks at $2\Theta = 34.4$ and 36.2° were due to the presence of ZnO crystals,[67] formed via oxidation of zinc originally present on the galvanized steel cathode surface.[68] Finally,

peaks that are present in some products at $2\Theta = 43.5$ and 44.7° are due to the NiO crystal lattice[69,70] and Ni electrodeposited onto the product on the cathode from the molten salt solution, respectively. It has been noted previously that zinc and nickel ion admixtures to the molten carbonates mediate the synthesis and contribute to the yield of carbon nanotubes in the process of CO_2 electrolysis.[7,10]

The products of CO_2 electrolysis were further visualized by means of transmission and scanning electron microscopy (TEM and SEM, Fig. 14). Images demonstrated multiwalled CNT (MWCNT) obtained in all borate/carbonate compositions at 550 °C. The MWCNT possessed 10–16 graphene layers, with walls approximately 4.5–5 nm thick, and diameters of ~15.5 nm. Similar MWCNT have been observed previously in the products of CO_2 electrolysis conducted in alkali metal carbonates only, without borates.[7,10]

Raman spectra of our electroreduction products (Fig. 15) showed a strong peak at around 1580 cm^{-1} (G-band, arising from the sp^2 carbon stretching of the C–C bond) and an additional band at 1350 cm^{-1} (D-band caused by the disordered structure of graphene). The presence of the G-band Raman feature is typical of all graphite-like materials, including multiwall CNT.[71,72] The presence of the peak at around 2690 cm^{-1}, corresponding to the G′ band, is more specific to small crystallites in CNT. The G-peak of the products prepared in 75 mol% initial borate composition was somewhat broader than the one observed in the spectra of the product obtained in the 1 : 1 borate/carbonate blend (borate content, 50 mol%), and some splitting of the G-peak into two peaks, centered at 1585 cm^{-1} and 1610 cm^{-1} (D′-peak) was apparent. This can be explained by the presence of the amorphous carbon impurities
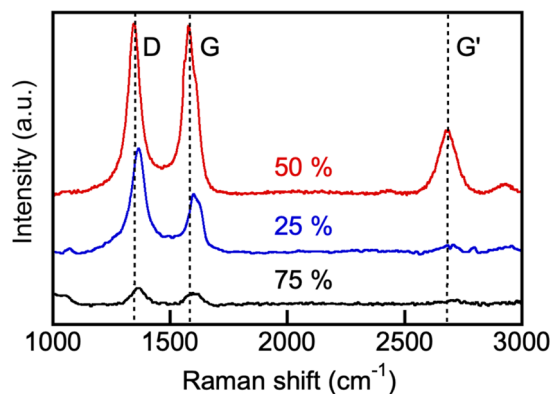
Fig. 14 TEM (a) and SEM (b) microphotographs of MWCNT found in the products of CO_2 electrolysis conducted in borate ($Li_{1.5}Na_{1.5}BO_3$) and eutectic carbonate ($Li_{1.24}K_{0.76}CO_3$) blend (1 : 1 mol/mol) at 550 °C.

on the graphitic layers of the CNT, which were observed by SEM. Overall, Raman spectra (Fig. 15), together with the XRD (Fig. 13) and electron microscopy (Fig. 14), provide unequivocal evidence of the presence of carbon nanotubes in the products of our CO_2 electroreduction process.

Fig. 15 Raman spectra of the products of CO_2 electrolysis conducted in borate ($Li_{1.5}Na_{1.5}BO_3$) and eutectic carbonate ($Li_{1.24}K_{0.76}CO_3$) blends at 550 °C. Numbers indicate the initial borate concentration in the blend (mol%). For other detail, see Experimental.

Conclusions

A family of blended compositions of molten alkali metal borates and carbonates has been examined as reversible CO_2 absorbents as well as media for the CO_2 electrolysis for carbon conversion. Salt structure, reactions with CO_2 and viscosity were studied. Blended borate($Li_{1.5}Na_{1.5}BO_3$) and eutectic Li, K carbonate ($Li_{1.24}K_{0.76}CO_3$) compositions are molten in the 550–600 °C (medium) temperature range. These compositions can be applied as reversible molten absorbents of CO_2, without a significant deterioration of the capture capacity over many cycles of the pressure swing operation. Addition of carbonates to the molten borate lowers overall CO_2 uptake due to the lower sorption capacity of carbonate. However, the addition of eutectic carbonates to the molten Li, Na borate (i) lowers the melt viscosity and enables lowering of the temperature of the pressure swing operation as well as (ii) dramatically accelerates the CO_2 uptake at the initial stage of the cycle, potentially enabling a faster cycling. Blended borate/carbonate compositions were found that possess simultaneous maximum loading capacity for CO_2 and enable maximum product (multiwall carbon nanotube) yield at medium temperatures (550°).

The blended borate/carbonate compositions described herein can find utility in processes involving both carbon capture and CO_2 capture/utilization applications. For the reversible capture plant design, the most influential parameters are the cost of CO_2 handling (transport and storage), the cost of electricity, and the energy required for the separation.[19] For the CCUS processes involving both capture and conversion designs, the cost of electricity is the most important factor. Given that a very large amount of electrical energy is required for this design, it must be supplied by renewable energy.[5,73] The high coulombic efficiency (over 90%, Fig. 12) achieved with some of the borate/carbonate blends is also a very influential factor. Our future efforts will focus on the search for the cost-optimum molten salt materials for CCUS in the medium to low temperature ranges.

Conflicts of interest

There are no conflicts to declare.

Acknowledgements

References

1 W. Weng, B. Jiang, Z. Wang and W. Xiao, *Sci. Adv.*, 2020, **6**(9), eaay9278, DOI: **10.1126/sciadv.aay9278**.

2   S. Jing, M. Wang and W. Xiao, *J. Energy Chem.*, 2022, **64**, 404, DOI: **10.1016/j.jechem.2021.05.012**.

3   W. Weng, L. Tang and W. Xiao, *J. Energy Chem.*, 2019, **28**, 128, DOI: **10.1016/j.jechem.2018.06.012**.

4   S. Licht, X. Liu, G. Licht, X. Wang, A. Swesi and Y. Chan, *Mater. Today Sustainability*, 2019, **6**, 100023.

5   J. Ren, A. Yu, P. Peng, M. Lefler, F.-F. Li and S. Licht, *Acc. Chem. Res.*, 2019, **52**(11), 3177, DOI: **10.1021/acs.accounts.9b00405**.

6   S. Licht, Carbon dioxide to carbon nanotube scale-up, arXiv, 2017, preprint, arXiv:1710.07246.

7   J. Ren and S. Licht, *Sci. Rep.*, 2016, **6**, 27760.

8   X. Chen, Z. Zhao, J. Qu, B. Zhang, X. Ding, Y. Geng, H. Xie, D. Wang and H. Yin, *ACS Sustainable Chem. Eng.*, 2021, **9**, 4167, DOI: **10.1021/acssuschemeng.1c00028**.

9   X. Wang, X. Liu, G. Licht, B. Wang and S. Licht, *J. CO2 Util.*, 2019, **34**, 303, DOI: **10.1016/j.jcou.2019.07.007**.

10 J. Johnson, M. Ren, G. Lefler, G. Licht, J. Vicini, X. Liu and S. Licht, *Mater. Today Energy*, 2017, **5**, 230, DOI: **10.1016/j.mtener.2017.07.003**.

11 T. Harada and T. A. Hatton, Carbon dioxide removal using lithium borate, *US Patent*, 10913658, 2021.

12 T. Harada, C. Halliday, A. Jamal and T. A. Hatton, *J. Mater. Chem. A*, 2019, **7**, 21827, DOI: **10.1039/C9TA09122J**.

13 T. Harada and T. A. Hatton, *J. Mater. Chem. A*, 2017, **5**, 22224, DOI: **10.1039/C7TA06167F**.

14 C. Halliday, N. Ozbek and T. A. Hatton, *ACS Appl. Mater. Interfaces*, 2020, **12**, 51468, DOI: **10.1021/acsami.0c14633**.

15 C. Halliday, T. Harada and T. A. Hatton, *Ind. Eng. Chem. Res.*, 2020, **59**, 8937, DOI: **10.1021/acs.iecr.0c01140**.

16 C. Halliday, T. Harada and T. A. Hatton, *Environ. Sci. Technol.*, 2020, **54**, 6319, DOI: **10.1021/acs.est.0c01671**.

17 C. Halliday, T. Harada and T. A. Hatton, *Chem. Mater.*, 2019, **32**, 348, DOI: **10.1021/acs.chemmater.9b03876**.

18 C. Halliday and T. A. Hatton, *Ind. Eng. Chem. Res.*, 2021, **60**(26), 9313, DOI: **10.1021/acs.iecr.1c00597**.

19 C. Halliday and T. A. Hatton, *Appl. Energy*, 2020, **280**, 116016, DOI: **10.1016/j.apenergy.2020.116016**.

20 S. W. Martin, E. I. Cooper and C. A. Angell, *J. Am. Ceram. Soc.*, 1983, **66**, c153, DOI: **10.1111/j.1151-2916.1983.tb10622.x**.

21 M. P. Nitzsche, L. Bromberg and T. A. Hatton, Capture and electrochemical conversion of CO_2 into carbon nanotubes using molten alkali metal borates, *Amer. Chem. Soc. Fall Meeting*, Chicago, IL, 08.21.2022.

22 J. Ren, J. Lau, M. Lefler and S. Licht, *J. Phys. Chem. C*, 2015, **119**, 23342, DOI: **10.1021/acs.jpcc.5b07026**.

23 H. Yin, X. Mao, D. Tang, W. Xiao, L. Xing, H. Zhu, D. Wang and D. R. Sadoway, *Energy Environ. Sci.*, 2013, **6**, 1538–1545, DOI: **10.1039/C3EE24132G**.

24 X. Liu, G. Licht, X. Wang and S. Licht, *Catalysts*, 2022, **12**, 137, DOI: **10.3390/catal12020137**.

25 H. V. Ijije, R. C. Lawrence and G. Z. Chen, *RSC Adv.*, 2014, **4**, 35808, DOI: **10.1039/C4RA04629C**.

26 C. Chen, T. Tran, R. Olivares, S. Wright and S. Sun, *J. Sol. Energy Eng.*, 2014, **136**(3), 031017, DOI: **10.1115/1.4027264**, (7 pages).

27 G. J. Janz and M. R. Lorenz, *J. Chem. Eng. Data*, 1961, **6**(3), 321, DOI: **10.1021/je00103a001**.

28 G. Argandoña, M. Aresti, J. M. Blanco, E. Muel and J. Esarte, *Appl. Sci.*, 2021, **11**, 7597, DOI: **10.3390/app11167597**.

29 M. Loubser, C. Strydom and H. A. Potgieter, *X-Ray Spectrom.*, 2004, **33**, 212, DOI: **10.1002/xrs.700**.

30 X. Wang, X. Liu, G. Licht and S. Licht, *Sci. Rep.*, 2020, **10**, 15146, DOI: **10.1038/s41598-020-71644-0**.

31 L. Hu, B. Deng, K. Du, R. Jiang, Y. Dou and D. Wang, *iScience*, 2020, **23**, 101607, DOI: **10.1016/j.isci.2020.101607**.

32 L. Hu, B. Deng, Z. Yang and D. Wang, *Electrochem. Commun.*, 2020, **121**, 106864, DOI: **10.1016/j.elecom.2020.106864**.

33 N. Khalizadeh, E. B. Saion, H. Mirabolghasemi, A. H. B. Shaari, M. B. Hashim, M. B. H. Ahmad, N. M. Ali and A. Dehzangi, *J. Mater. Res. Technol.*, 2016, **5**, 37, DOI: **10.1016/j.jmrt.2015.05.005**.

34 F. Claisse, *Powder Diffr.*, 2006, **21**(2), 181, DOI: **10.1154/1.2219872**.

35 E. Braysher, B. Russell, S. Woods, M. García-Miranda, P. Ivanov and D. Read, *J. Radioanal. Nucl. Chem.*, 2019, **321**, 183, DOI: **10.1007/s10967-019-06572-z**.

36 Y. Anzai, K. Terashima and S. Kimura, *J. Cryst. Growth*, 1993, **134**, 235, DOI: **10.1016/0022-0248(93)90131-F**.

37 J. Filipiak, A. Majchrowski and T. Łukasiewicz, *Arch. Acoust.*, 1994, **19**, 131 **https://acoustics.ippt.pan.pl/index.php/aa/article/view/1067/904**.

38 K. Byrappa and K. V. K. Shekar, Phases and crystallization in the system Li2O-B2O3-H$_2$O under hydrothermal conditions, *J. Mater. Res.*, 1993, **8**, 864–870, DOI: **10.1557/JMR.1993.0864**.

39 P. J. Bray, S. A. Feller, G. E. Jellison and Y. H. Yun, *J. Non-Cryst. Solids*, 1980, **39**, 93, DOI: **10.1016/0022-3093(80)90400-7**.

40 A. Senyshyn, B. Schwarz, T. Lorenz, V. T. Adamiv, Y. V. Burak, J. Banys, R. Grigalaitis, L. Vasylechko, H. Ehrenberg and H. Fuess, *J. Appl. Phys.*, 2010, **108**, 093524, DOI: **10.1063/1.3504244**.

41 B. Chen, U. Werner-Zwanziger, M. L. F. Nascimento, L. Ghussn, E. D. Zanotto and J. W. Zwanziger, *J. Phys. Chem. C*, 2009, **113**, 20725, DOI: **10.1021/jp907259e**.

42 D. Di Genova, C. Cimarelli, K.-U. Hess and D. B. Dingwell, *Am. Mineral.*, 2016, **101**, 953, DOI: **10.2138/am-2016-5537CCBYNCND**.

43 S. W. Kim, K. Uematsu, K. Toda and M. Sato, *J. Ceram. Soc. Jpn*, 2015, **143**, 355, DOI: **10.2109/jcersj2.123.355**.

44 G. J. Janz and J. Saegusa, *J. Electrochem. Soc.*, 1963, **110**, 452, DOI: **10.1149/1.2425785**.

45 T. Harada, F. Simeon, E. Z. Hamad and T. A. Hatton, *Chem. Mater.*, 2015, **27**(6), 1943, DOI: **10.1021/cm503295g**.

46 W. Gao, M. A. Vasiliades, C. M. Damaskinos, M. Zhao, W. Fan, Q. Wang, T. R. Reina and A. M. Efstathiou, *Environ. Sci. Technol.*, 2021, **55**(8), 4513, DOI: **10.1021/acs.est.0c08731**.

47 T. J. W. D. Bruijn, W. A. D. Jong and P. J. V. D. Berg, *Thermochim. Acta*, 1981, **45**, 315–325, DOI: **10.1016/0040-6031(81)85091-5**.

48 A. Khawam and D. R. Flanagan, *J. Phys. Chem. B*, 2006, **110**, 17315, DOI: **10.1021/jp062746a**.

49 M. Lefler and C. L. Pint, *ACS Cent. Sci.*, 2016, **2**, 162, DOI: **10.1021/acscentsci.5b00400**.

50 J. Ren, F.-F. Li, J. Lau, L. González-Urbina and S. Licht, *Nano Lett.*, 2015, **15**, 6142, DOI: **10.1021/acs.nanolett.5b02427**.

51 S. Licht, B. Wang, S. Ghosh, H. Ayub, D. Jiang and J. Ganley, *J. Phys. Chem. Lett.*, 2010, **1**, 2363, DOI: **10.1021/jz100829s**.

52 Z. Li, D. Yuan, H. Wu, W. Li and D. Gu, *Inorg. Chem. Front.*, 2018, **5**, 208, DOI: **10.1039/C7QI00479F**.

53 V. N. Tare and J. B. Wagner, *J. Appl. Phys.*, 1983, **54**, 6459, DOI: **10.1063/1.331927**.

54 S. M. A. Shibli, B. N. Meena and R. Remya, *Surf. Coat. Technol.*, 2015, **262**, 210, DOI: **10.1016/j.surfcoat.2014.12.054**.

55 P. Wang, Y. Liu, Z. Li, D. Ji, Z. Qiao, J. Zhang, Q. Jia and H. Wu, *J. Electrochem. Soc.*, 2021, **168**, 083501, DOI: **10.1149/2.0861910jes**.

56 F. M. Chang, S. Brahma, J. H. Huang, Z. Z. Wu and K.-Y. Lo, *Sci. Rep.*, 2019, **9**, 905, DOI: **10.1038/s41598-018-37601-8**.

57 R. Wartena, J. Winnick and P. H. Pfromm, *J. Appl. Electrochem.*, 2002, **32**, 415, DOI: **10.1023/A:1016334307899**.

58 Y. Izaki, Y. Mugikura, T. Watanabe, M. Kawase and J. R. Selman, *J. Power Sources*, 1998, **75**, 236, DOI: **10.1016/S0378-7753(98)00117-7**.

59 M. D. Ingram and G. I. Janz, *Electrochim. Acta*, 1965, **10**, 783, DOI: **10.1016/0013-4686(65)80043-3**.

60 M. S. Yazici and J. R. Selman, *J. Electroanal. Chem.*, 1998, **457**, 89, DOI: **10.1016/S0022-0728(98)00126-0**.

61 J. P. T. Vossen, L. Plompand and J. H. W. de Wit, *J. Electrochem. Soc.*, 1994, **141**, 3040, DOI: **10.1149/1.2059276**.

62 Q. Li, F. Borup, I. Petrushina and N. Bjerrum, *J. Electrochem. Soc.*, 1999, **146**, 2449, DOI: **10.1149/1.1391954**.

63 B. D. Che, B. Q. Nguyen, B. Q. Nguyen, L. T. Nguyên, L. T. Nguyên and N. H. Nguyen, *Chem. Cent. J.*, 2015, **9**, 10, DOI: **10.1186/s13065-015-0087-2**.

64 G. Xu, Z.-C. Feng, Z. Popovic, J.-Y. Lin and J. J. Vittal, *Adv. Mater.*, 2001, **13**, 264, DOI: **10.1002/1521-4095(200102)13:4<264**.

65 D. N. Futaba, T. Yamada, K. Kobashi, M. Yumura and K. Hata, *J. Am. Chem. Soc.*, 2011, **133**, 5716, DOI: **10.1021/ja2005994**.

66 W. Cai, R. Chen, Y. Yang, M. Yi and L. Xiang, *Crystals*, 2018, **8**, 19, DOI: **10.3390/cryst8010019**.

67 JCPDS #79-0206, #36-1451.

68 P. Rajasekaran, H. Kannan, S. Das, M. Young and S. Santra, *AIMS Environ. Sci.*, 2016, **3**, 439, DOI: **10.3934/environsci.2016.3.439**.

69 S. Rakshit, S. Ghosh, S. Chall, S. S. Mati, S. P. Moulik and S. C. Bhattacharya, *RSC Adv.*, 2013, **3**, 19348, DOI: **10.1039/C3RA42628A**.

70 V. D. Jović, V. Maksimović, M. G. Pavlović and K. I. Popov, *J. Solid State Electrochem.*, 2006, **10**, 373, DOI: **10.1007/s10008-005-0687-1**.

71 E. F. Antunes, A. O. Lobo, E. J. Corat, V. J. Trava-Airoldi, A. A. Martin and C. Verissimo, *Carbon*, 2006, **44**, 2202, DOI: **10.1016/j.carbon.2006.03.003**.

72 M. S. Dresselhaus, A. Jorio, M. Hofmann, G. Dresselhaus and R. Saito, *Nano Lett.*, 2010, **10**, 751, DOI: **10.1021/nl904286r**.

73 S. Licht, arXiv, 2019, preprint, arXiv:1901.07134.